

A figure of merit for efficiency roll-off in TADF-based organic LEDs

<https://doi.org/10.1038/s41586-024-07149-x>

S. Diesing^{1,2,3}, L. Zhang^{1,2,3}, E. Zysman-Colman²✉ & I. D. W. Samuel^{1,3}✉

Received: 31 March 2023

Accepted: 1 February 2024

Published online: 27 March 2024

Open access

 Check for updates

Organic light-emitting diodes (OLEDs) are a revolutionary light-emitting display technology that has been successfully commercialized in mobile phones and televisions^{1,2}. The injected charges form both singlet and triplet excitons, and for high efficiency it is important to enable triplets as well as singlets to emit light. At present, materials that harvest triplets by thermally activated delayed fluorescence (TADF) are a very active field of research as an alternative to phosphorescent emitters that usually use heavy metal atoms^{3,4}. Although excellent progress has been made, in most TADF OLEDs there is a severe decrease of efficiency as the drive current is increased, known as efficiency roll-off. So far, much of the literature suggests that efficiency roll-off should be reduced by minimizing the energy difference between singlet and triplet excited states (ΔE_{ST}) to maximize the rate of conversion of triplets to singlets by means of reverse intersystem crossing (k_{RISC})^{5–20}. We analyse the efficiency roll-off in a wide range of TADF OLEDs and find that neither of these parameters fully accounts for the reported efficiency roll-off. By considering the dynamic equilibrium between singlets and triplets in TADF materials, we propose a figure of merit for materials design to reduce efficiency roll-off and discuss its correlation with reported data of TADF OLEDs. Our new figure of merit will guide the design and development of TADF materials that can reduce efficiency roll-off. It will help improve the efficiency of TADF OLEDs at realistic display operating conditions and expand the use of TADF materials to applications that require high brightness, such as lighting, augmented reality and lasing.

Organic light-emitting diodes (OLEDs) are now widely used in displays and are being developed for applications in lighting, sensing and communications^{1,2}. They consist of layers of charge transporting and light-emitting organic semiconductors in between two electrodes, at least one of which is transparent. When the injected charges recombine, they form both singlet and triplet excitons. Spin statistics suggest three triplets form for each singlet, a ratio that has been verified for evaporated OLEDs using low molecular weight emitters²¹. In OLEDs using fluorescent materials, only the singlets emit light. Phosphorescent OLED materials were therefore developed to obtain light emission from the triplets as well²². These work very well for red and green emission, but there is not yet a blue phosphorescent emitter meeting all commercial requirements²³. Consequently, there is currently great interest in thermally activated delayed fluorescence (TADF) as an alternative approach to obtaining light from triplets^{3,4}. Following the pioneering work of Adachi and coworkers in 2011, there have been more than 4,000 papers with the keyword thermally activated delayed fluorescence^{24,25} (based on results from 16 February 2024 that mention thermally activated delayed fluorescence or TADF since 2011).

A problem in both organic and inorganic LEDs is that as the drive current is increased for more light output, the efficiency decreases²⁶. This is known as efficiency roll-off and is illustrated in Fig. 1a, which shows the efficiency as a function of current density for prototypical examples of fluorescent, phosphorescent and TADF OLEDs^{3,27,28}.

Figure 1a shows that the phosphorescent and TADF OLEDs have more than four times the efficiency of the fluorescent OLEDs, but that their efficiency decreases and particularly severely for the TADF OLEDs as the current density is increased. To compare the behaviour of a wide range of OLEDs of each type, we define J_{90} as the current density at which the external quantum efficiency (EQE) falls to 90% of its peak value, as illustrated in Fig. 1b.

We have extracted J_{90} from published data on a wide range of OLEDs together with their EQE at a practical luminance of 1,000 cd m⁻². These are plotted for each class of OLEDs and each colour in Fig. 1c. The ideal behaviour would be high J_{90} (for low efficiency roll-off) and high EQE: that is, the top right quadrant of the graph. Most fluorescent OLEDs fall in the green rectangle (A), which is a region of high J_{90} but low EQE. Most phosphorescent OLEDs (and a few others) fall in the blue rectangle (B). The upper half of this rectangle represents OLEDs with high efficiency and fairly high J_{90} . TADF OLEDs fall mainly in region C. Notably, there is a much wider spread of both EQE and J_{90} than for the other classes of OLEDs, possibly because TADF OLEDs is a much younger field. The upper right part of region C shows that there are some reports of TADF OLEDs with high EQE and moderately high J_{90} , although lower than for good phosphorescent devices. However, region C also extends to extremely low values of J_{90} , that is, there are many TADF devices experiencing significant efficiency roll-off at current densities below 0.1 mA cm⁻². Even for a green device, this would correspond

¹Organic Semiconductor Centre, SUPA, School of Physics and Astronomy, University of St Andrews, St Andrews, UK. ²Organic Semiconductor Centre, EaStCHEM, School of Chemistry, St Andrews, UK. ³These authors contributed equally: S. Diesing, L. Zhang, I. D. W. Samuel. ✉e-mail: eli.zysman-colman@st-andrews.ac.uk; idws@st-andrews.ac.uk

Analysis

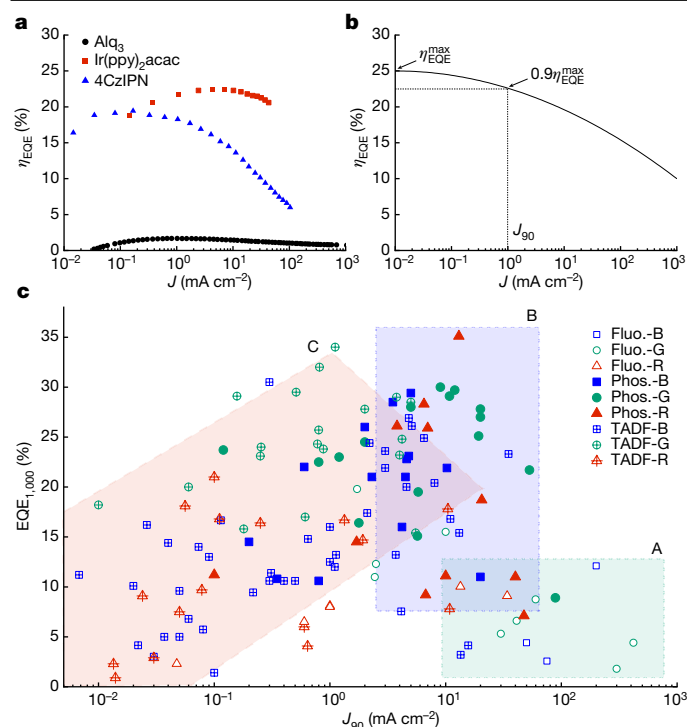


Fig. 1 | Examples of efficiency roll-off. **a**, Efficiency roll-off of prototypical fluorescent (Alq_3), phosphorescent ($\text{Ir}(\text{ppy})_2\text{acac}$) and TADF (4CzIPN) OLEDs^{3,27,28}. **b**, Schematic graph showing definition of J_{90} . **c**, Graph of the relation between J_{90} and $\text{EQE}_{1,000}$ for TADF^{5,38,39,48–113}, fluorescent (Fluo.)^{28,114–129} and phosphorescent (Phos.)^{86–88,128–155} devices emitting in the red (R), green (G) and blue (B) regions of the spectrum (for the references, see Methods).

to a brightness of at most 100 cd m^{-2} , whereas typical displays run at 400 cd m^{-2} and their individual pixels often run at much higher brightness to achieve an average 400 cd m^{-2} on the display²⁹. Hence, many reported TADF OLEDs have severe efficiency roll-off and even the best have significant efficiency roll-off (J_{90} of a few mA cm^{-2}).

Efficiency roll-off in TADF devices

This brings us to the central question of this analysis, which is, what can be done in terms of emitter design to reduce efficiency roll-off (that is, increase J_{90})? In other words, which photophysical processes need to be tuned by molecular design to minimize inherent limitations of the emitter that contribute to efficiency roll-off? Efficiency roll-off arises both from the emitter design and the device design, but for an optimized device design (for example, balanced charge carriers and wide recombination zone) it will ultimately be limited by the properties of the emitter.

To identify the crucial parameters for emitter design, we first need to consider what causes efficiency roll-off. Studies in phosphorescent OLEDs have shown that triplet–triplet annihilation (TTA) and triplet–polaron annihilation (TPA) are the main loss mechanisms as the current density is increased^{29–31}. A similar understanding is developing in TADF OLEDs in which TTA, TPA and singlet–triplet annihilation (STA) may all contribute^{32–34}. These are all bimolecular processes and thus much more severe at higher excitation densities. Furthermore, as all these processes involve triplets, they can be mitigated by reducing the triplet lifetime and hence reducing the triplet population. This has been achieved successfully in phosphorescent OLEDs by engineering the light-emitting material (for example, by using an iridium complex) to show a large radiative rate constant from the triplet state and thus achieving a relatively short triplet lifetime of around $1 \mu\text{s}$.

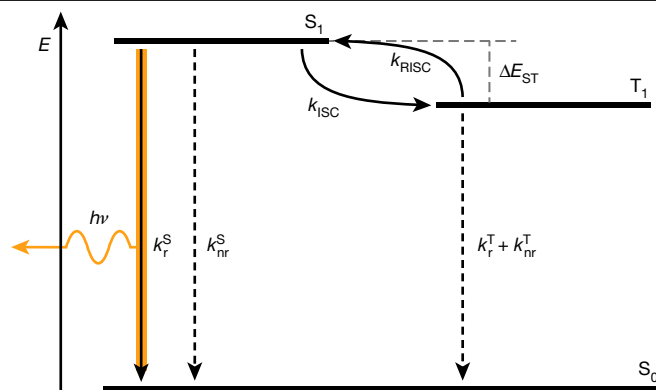


Fig. 2 | Simplified Jablonski diagram of a TADF emitter. The excited singlet and triplet states S_1 and T_1 , respectively, are shown in equilibrium due to the occurrence of both intersystem crossing (k_{ISC}) and reverse intersystem crossing (k_{RISC}) enabled by the small energy gap (ΔE_{ST}) between S_1 and T_1 . A TADF OLED emits light by radiative decay from S_1 (k_r^S), whereas non-radiative decay from both S_1 (k_{nr}^S) and T_1 (k_{nr}^T), as well as the negligible radiative decay from T_1 (k_r^T) are other deactivation pathways of excited species.

For comparison, delayed fluorescence lifetimes in organic TADF materials range from $1 \mu\text{s}$ to beyond $500 \mu\text{s}$. We briefly note that as well as reducing efficiency, bimolecular processes involving triplets are also a main mechanism of device degradation, providing a further reason to reduce the triplet population in operating devices³⁵.

Hence to reduce efficiency roll-off, we need to reduce triplet lifetime or, more precisely, the triplet population during device operation. This, however, is not as simply achieved as in the case of phosphorescence. The key photophysical processes in a TADF emitter are shown in Fig. 2. Singlets are converted to triplets via intersystem crossing (ISC) with rate constant k_{ISC} , and triplets to singlets via reverse intersystem crossing (RISC) at rate constant k_{RISC} . There is potentially radiative and non-radiative decay of both triplets and singlets, although in a good TADF material k_r^S will be much larger than any of k_{nr}^S , k_r^T and k_{nr}^T (refs. 36,37). The main approach advocated in the literature for reducing efficiency roll-off is to increase k_{RISC} , commonly by reducing the energy difference between singlet and triplet excited states (ΔE_{ST}) through molecular design by reducing the exchange integral between the highest occupied and lowest unoccupied molecular orbitals. In addition, there have been other attempts to increase k_{RISC} , for example by the use of heavy atoms, to increase spin–orbit coupling (SOC)^{5,38}. The emphasis on k_{RISC} is so strong that since 2016 there have been 16 publications in the *Nature* family alone exploring k_{RISC} (refs. 5–20). However, the expected improvement in J_{90} has not always materialized.

To understand how J_{90} depends on k_{RISC} , we have plotted the graph shown in Fig. 3. There is some correlation (Spearman correlation $\rho = 0.638$) in so far as there is a tendency towards higher J_{90} for higher k_{RISC} , but there is an enormous spread of the data (considering this is a log–log plot). For example, the blue dashed rectangle shows that J_{90} of roughly 2 mA cm^{-2} can be achieved with k_{RISC} from 2 to $20 \times 10^5 \text{ s}^{-1}$. The insufficiency of k_{RISC} as a guide for molecular design is vividly demonstrated by the red dashed rectangle that shows J_{90} for molecules designed with a high k_{RISC} of 8 – $15 \times 10^5 \text{ s}^{-1}$. The values of J_{90} range from 0.03 to 40 mA cm^{-2} , that is, by more than three orders of magnitude, showing k_{RISC} alone is inadequate as a predictor of efficiency roll-off.

Derivation of FOM

To develop guidelines for TADF materials design to reduce efficiency roll-off in OLEDs, we should first look more closely at Fig. 2 and the mechanism of TADF.

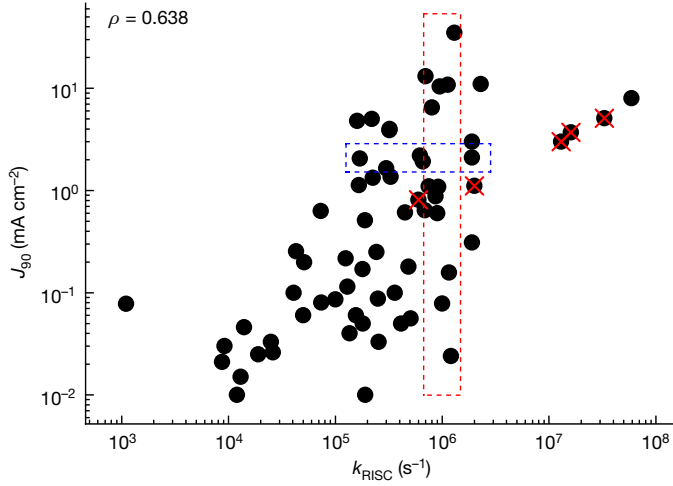


Fig. 3 | Data analysis. J_{90} of the reported TADF OLEDs with respect to k_{RISC} (Spearman correlation $\rho = 0.638$). Red crosses present TADF molecules containing heavy atoms that benefit from enhanced SOC to increase k_{RISC} . Data inside the dashed boxes are for comparison.

The physics of TADF is often studied using transient photoluminescence (PL) measurements in which the emitter is excited using a laser pulse. Excitons are generated in the excited singlet state (S_1), and the decay of the excited state is slowed by cycling to and from the triplet state (T_1) by ISC and RISC, respectively. In an OLED, charge injection leads to a buildup of both S_1 (25%) and T_1 (75%) excitons as well as polarons. There is a dynamic equilibrium between S_1 and T_1 facilitated by the ISC/RISC cycling. To ascertain on which side the dynamic equilibrium lies, an equilibrium constant K_{eq} is defined as

$$K_{\text{eq}} = \frac{[S_1]}{[T_1]} \quad (1)$$

For a three-level TADF OLED under low constant current electrical excitation, the equilibrium constant is given as follows (see Methods for the derivation)

$$K_{\text{eq}} = \frac{3k_{\text{RISC}} + k^{\text{T}}}{3k^{\text{S}} + k_{\text{ISC}}}, \quad (2)$$

where k^{S} is the sum of the rate constants for ISC (k_{ISC}), radiative (k_r^{S}) and non-radiative (k_{nr}^{S}) decay from S_1 , and k^{T} is the sum of the rate constants for RISC (k_{RISC}), radiative (k_r^{T}) and non-radiative (k_{nr}^{T}) decay from T_1 . As explained earlier, to minimize the EQE roll-off a low T_1 population is necessary to suppress TTA and to a lesser extent STA and TPA. For an OLED operated at high brightness this translates to the requirement of maximizing the S_1 population relative to the T_1 population, which can be achieved by maximizing K_{eq} . Furthermore, according to Le Chatelier's principle, an equilibrium can be moved to a desired product by removing the product from the equilibrium. Here, the radiative decay of S_1 excitons is the desired product. Therefore, to minimize the fraction of triplet excitons in the steady-state OLED emitters should be developed (or selected) to maximize the product of radiative rate constant and equilibrium constant. In a good OLED, nearly all electrically excited excitons decay radiatively, that is $k_{\text{nr}}^{\text{S}} = k_{\text{nr}}^{\text{T}} = 0$. Thus, for a TADF emitter with photoluminescence quantum yield near unity and no phosphorescence contribution ($k_r^{\text{T}} = 0$), which is reasonable for good organic emitters, a figure of merit (FOM) for efficiency roll-off can be formulated as

$$k_r^{\text{S}} K_{\text{eq}} = \frac{4k_r^{\text{S}} k_{\text{RISC}}}{3k_r^{\text{S}} + 4k_{\text{ISC}}}. \quad (3)$$

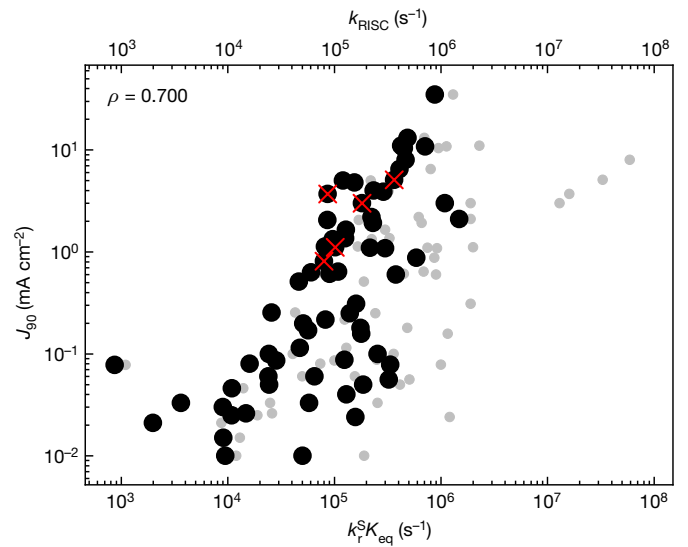


Fig. 4 | FOM. Correlations between J_{90} and $k_r^{\text{S}} K_{\text{eq}}$ with a Spearman correlation coefficient of $\rho = 0.700$. Red crosses identify TADF molecules containing heavy atoms that enhance SOC, which leads to an increase in k_{RISC} . In grey circles, the correlation of J_{90} and k_{RISC} from Fig. 3 is shown for comparison.

Figure 4 shows J_{90} plotted as a function of this FOM. There is a stronger correlation with J_{90} ($\rho = 0.700$) than k_{RISC} with J_{90} ($\rho = 0.638$). Higher $k_r^{\text{S}} K_{\text{eq}}$ leads to higher J_{90} . Accordingly, maximizing $k_r^{\text{S}} K_{\text{eq}}$ and thus minimizing the T_1 population under electrical excitation is a better strategy for improving efficiency roll-off than considering k_{RISC} alone. Figure 4 compares efficiency roll-off as a function of our FOM (black circles) with efficiency roll-off as a function of k_{RISC} (small grey circles). The FOM has a narrower spread of values as would be expected for the improved correlation.

It is interesting to apply this FOM to recent attempts to increase k_{RISC} by incorporating heavy atoms into the molecule to increase SOC^{5,38}. These studies are shown by red crosses in Figs. 3 and 4. This strategy is broadly successful at leading to fast k_{RISC} but does not necessarily lead to the highest J_{90} as k_{ISC} also increases, or k_r^{S} decreases. This interplay between these parameters is captured by the FOM as can be seen from the red crosses in Fig. 4 being in the same region as other materials. At the same time, incorporation of these larger atoms that result in weaker bonds also leads to faster non-radiative pathways and potentially poor device stability. Here, we can see that k_{RISC} and the proposed FOM give distinct assessments of the heavy atom approach, and that the latter is a better predictor of J_{90} for future molecular design. Another possible guide for design is (as for phosphorescent devices) short delayed fluorescence lifetime (τ_{DF})³⁹. The correlation of J_{90} with τ_{DF} is shown in Extended Data Fig. 1a. There is a good correlation ($\rho = -0.685$), although still some scatter. Actually, τ_{DF} has a much stronger correlation with the proposed FOM ($\rho = -0.801$) than with k_{RISC} ($\rho = -0.709$). In other words, the proposed FOM not only predicts the efficiency roll-off, but also clarifies the key physical processes that need to be optimized to achieve low efficiency roll-off. Although measuring τ_{DF} would be an effective way of screening materials for low potential efficiency roll-off after they have been synthesized, our FOM gives more insight into how to design a material for low efficiency roll-off by showing the exact combination of rate constants that should be optimized.

For many TADF materials k_{ISC} is substantially faster than k_r^{S} , in which case the FOM can be simplified to

$$k_r^{\text{S}} K_{\text{eq}} \approx \frac{k_r^{\text{S}} k_{\text{RISC}}}{k_{\text{ISC}}} \quad \text{for } k_r^{\text{T}} = k_{\text{nr}}^{\text{T}} = k_{\text{nr}}^{\text{S}} = 0 \text{ and } k_{\text{ISC}} \gg k_r^{\text{S}} \quad (4)$$

Analysis

This simplified FOM highlights the competition between k_{ISC} , k_{RISC} and k_{r}^{S} very clearly. It is equivalent to $k_{\text{r}}^{\text{S}}K_{\text{eq}}$ in the regime where k_{r}^{S} is smaller than k_{ISC} (Extended Data Fig. 2).

Other factors affecting efficiency roll-off

Although there is a good correlation between J_{90} and the proposed FOM, there is a significant spread of data points in Fig. 4. This can be understood to arise because efficiency roll-off involves a combination of the intrinsic properties of the emitting molecule with the extrinsic properties of the device. An analogous situation exists when using photoluminescence quantum yield as a predictor of device efficiency: whether a material realizes its full potential also depends on the device. Similarly, our FOM describes the best that could be achieved with a particular light-emitting material in a device limited by the triplet population. In real devices, many factors, especially imperfect charge balance, could lead to worse performance than this ideal case, and hence can explain the spread of the data in Fig. 4. In addition, at low current density some devices show efficiency increasing with current density, as can be seen for the devices in Fig. 1a. As J_{90} is taken as a reduction from peak efficiency, this will lead to higher values of J_{90} than in devices with peak efficiency at very low current. There is another example of this effect in Extended Data Fig. 3 that compares two 2CzPN devices^{3,40}. It should also be noted that practice for determining rate constants varies^{37,41}, which could also contribute to the spread.

Another important factor that could contribute to the spread of data is that the effect of a given triplet population depends on the material. In particular, reported TTA rate constants γ_{TT} are widely spread over eight orders of magnitude (10^{-18} – 10^{-10} $\text{cm}^3 \text{s}^{-1}$)^{32,33,42,43}. So, increasing the FOM will reduce triplet population, and is beneficial (increases J_{90}) but the improvement arising from the reduced triplet population depends on the value of γ_{TT} . Similar considerations apply to STA, in which again there is a range of γ_{ST} , and the relative importance of STA and TTA depends on the relative values of γ_{TT} and γ_{ST} . As these rate constants are not yet widely measured, we have not at this stage attempted to incorporate them into a FOM. However, we show their potential effect in Extended Data Fig. 4, which shows calculations of how J_{90} would depend on FOM for systems with k_{r}^{S} between 10^5 and 10^{10} s^{-1} , $k_{\text{ISC}}/k_{\text{r}}^{\text{S}}$ between 10^{-1} and 10^3 , and $k_{\text{r}}^{\text{S}}K_{\text{eq}}$ between 10^2 and 10^8 s^{-1} for a range of values of γ_{ST} , γ_{TT} and k_{r}^{S} . Extended Data Fig. 3a shows how for a given FOM, each order of magnitude change in γ_{TT} leads to an order of magnitude change in J_{90} . Extended Data Fig. 4b shows the potential interplay between TTA and STA. The J_{90} value behaves nearly linearly with $k_{\text{r}}^{\text{S}}K_{\text{eq}}$ when only TTA is considered (red dots, the slope is 2). If only STA is considered, there is still a correlation; however, at the same FOM, higher J_{90} is achieved when k_{r}^{S} is large. If both TTA and STA are significant, then the efficiency is limited by TTA at low FOM and by k_{r}^{S} at high FOM.

We also note that the kinetics of thin films can result in a multi-exponential transient PL, which is caused by conformational disorder⁴⁴. Such a decay can be analysed using a Laplace transformation of the three-level kinetics of each conformer⁴⁵. Our analysis does not include conformational disorder but could be applied in a similar manner to the analysis of multi-exponential transient PL caused by conformational disorder.

Conclusion

Our analysis has important implications for the rapidly growing field of TADF OLED development. At present, many such devices suffer such severe efficiency roll-off that they are unsuitable for practical application and, as we have shown, current emitter design focusing on maximizing k_{RISC} alone is not an effective strategy. On the basis of the insight from considering the quasi-equilibrium in TADF, we instead propose that the focus of materials design and development should

shift to maximizing a FOM that combines the physical processes that determine efficiency roll-off. Target values of the FOM will depend on the requirements of particular applications, as well as device design and severity of bimolecular effects. We estimate values of FOM required for materials with chromaticity close to the BT2020 standard⁴⁶, and with Gaussian emission spectra of width 15 nm in the blue, 30 nm in the green and 45 nm in the red. We use the calculation for Extended Data Fig. 4a with $\gamma_{\text{TT}} = 10^{-13} \text{ cm}^3 \text{ s}^{-1}$ and find the FOM required to achieve 90% of a peak EQE of 25% at a brightness of 1,000 cd m^{-2} . We find that for a deep blue emitter ($\lambda_{\text{max}} = 467 \text{ nm}$, CIE 1931 colour space (0.131, 0.049)) a FOM of at least $1.5 \times 10^5 \text{ s}^{-1}$ is required. For a green emitter ($\lambda_{\text{max}} = 529 \text{ nm}$, CIE (0.169, 0.772)) a FOM of $5.1 \times 10^4 \text{ s}^{-1}$ would be required, and for red ($\lambda_{\text{max}} = 650 \text{ nm}$, CIE (0.708, 0.292)) a FOM of at least $1.3 \times 10^5 \text{ s}^{-1}$ is needed.

In terms of material design for low efficiency roll-off, it is not necessary to maximize k_{RISC} , but it is very desirable to maximize k_{RISC} relative to k_{ISC} (without sacrificing k_{r}^{S}). It is also a useful strategy to seek materials with high k_{r}^{S} (providing $k_{\text{RISC}}/k_{\text{ISC}}$ is not reduced), which is also the underlying physics for hyperfluorescent OLEDs⁴⁷, where the rate constant of Förster resonance energy transfer takes the place of k_{r}^{S} in the FOM and lowers the triplet population on the TADF sensitizer. At the same time, there is a need to understand which process dominates the efficiency roll-off. Whereas all main annihilation processes scale with the triplet population and thus inversely with our proposed FOM, the relative importance of these processes in each OLED is not sufficiently known. Therefore, there is a need to measure both γ_{ST} and γ_{TT} in a wider set of devices to fully understand how the excited-state kinetics of the emitter need to be engineered to reduce efficiency roll-off.

We hope that our FOM and these insights will enable the field of TADF OLEDs to overcome the challenge of efficiency roll-off and advance more rapidly to applications in displays, lighting and beyond.

Online content

Any methods, additional references, Nature Portfolio reporting summaries, source data, extended data, supplementary information, acknowledgements, peer review information; details of author contributions and competing interests; and statements of data and code availability are available at <https://doi.org/10.1038/s41586-024-07149-x>.

- Forrest, S. R. The path to ubiquitous and low-cost organic electronic appliances on plastic. *Nature* **428**, 911–918 (2004).
- Hong, G. et al. A brief history of OLEDs-emitter development and industry milestones. *Adv. Mater.* **33**, e2005630 (2021).
- Uoyama, H., Goushi, K., Shizu, K., Nomura, H. & Adachi, C. Highly efficient organic light-emitting diodes from delayed fluorescence. *Nature* **492**, 234 (2012).
- Wong, M. Y. & Zysman-Colman, E. Purely organic thermally activated delayed fluorescence materials for organic light-emitting diodes. *Adv. Mater.* **29**, 1605444 (2017).
- Hu, Y. X. et al. Efficient selenium-integrated TADF OLEDs with reduced roll-off. *Nat. Photonics* **16**, 803–810 (2022).
- Cui, L.-S. et al. Fast spin-flip enables efficient and stable organic electroluminescence from charge-transfer states. *Nat. Photonics* **14**, 636–642 (2020).
- Wada, Y., Nakagawa, H., Matsumoto, S., Wakisaka, Y. & Kaji, H. Organic light emitters exhibiting very fast reverse intersystem crossing. *Nat. Photonics* **14**, 643–649 (2020).
- Luo, Y. et al. Ultra-fast triplet-triplet-annihilation-mediated high-lying reverse intersystem crossing triggered by participation of $\text{n}\pi^*$ -featured excited states. *Nat. Commun.* **13**, 6892 (2022).
- Gillett, A. J. et al. Dielectric control of reverse intersystem crossing in thermally activated delayed fluorescence emitters. *Nat. Mater.* **21**, 1150–1157 (2022).
- Aizawa, N., Harabuchi, Y., Maeda, S. & Pu, Y. J. Kinetic prediction of reverse intersystem crossing in organic donor-acceptor molecules. *Nat. Commun.* **11**, 3909 (2020).
- Zysman-Colman, E. Molecular designs offer fast exciton conversion. *Nat. Photonics* **14**, 593–594 (2020).
- Yu, Y., Mallick, S., Wang, M. & Börjesson, K. Barrier-free reverse-intersystem crossing in organic molecules by strong light-matter coupling. *Nat. Commun.* **12**, 3255 (2021).
- Stranius, K., Hertzog, M. & Borjesson, K. Selective manipulation of electronically excited states through strong light-matter interactions. *Nat. Commun.* **9**, 2273 (2018).
- Etherington, M. K., Gibson, J., Higginbotham, H. F., Penfold, T. J. & Monkman, A. P. Revealing the spin-vibronic coupling mechanism of thermally activated delayed fluorescence. *Nat. Commun.* **7**, 13680 (2016).

15. Schleper, A. L. et al. Hot exciplexes in U-shaped TADF molecules with emission from locally excited states. *Nat. Commun.* **12**, 6179 (2021).
16. Li, F. et al. Singlet and triplet to doublet energy transfer: improving organic light-emitting diodes with radicals. *Nat. Commun.* **13**, 2744 (2022).
17. Wu, X. et al. The role of host-guest interactions in organic emitters employing MR-TADF. *Nat. Photonics* **15**, 780–786 (2021).
18. Gillett, A. J. et al. Spontaneous exciton dissociation enables spin state interconversion in delayed fluorescence organic semiconductors. *Nat. Commun.* **12**, 6640 (2021).
19. Fan, X.-C. et al. Ultrapure green organic light-emitting diodes based on highly distorted fused π -conjugated molecular design. *Nat. Photonics* **17**, 280–285 (2023).
20. Zhao, W., He, Z. & Tang, B. Z. Room-temperature phosphorescence from organic aggregates. *Nat. Rev. Mater.* **5**, 869–885 (2020).
21. Segal, M., Baldo, M. A., Holmes, R. J., Forrest, S. R. & Soos, Z. G. Excitonic singlet-triplet ratios in molecular and polymeric organic materials. *Phys. Rev. B* **68**, 075211 (2003).
22. Baldo, M. A. et al. Highly efficient phosphorescent emission from organic electroluminescent devices. *Nature* **395**, 151–154 (1998).
23. Cai, X. & Su, S.-J. Marching toward highly efficient, pure-blue, and stable thermally activated delayed fluorescent organic light-emitting diodes. *Adv. Funct. Mater.* **28**, 1802558 (2018).
24. Endo, A. et al. Efficient up-conversion of triplet excitons into a singlet state and its application for organic light emitting diodes. *Appl. Phys. Lett.* **98**, 083302 (2011).
25. Citation Report (Web of Science, accessed 16 February, 2024); www.webofscience.com/wos/woscc/citation-report/ad524515-2457-4194-9799-2409c8bd955f-cc8165d0.
26. Murawski, C., Leo, K. & Gather, M. C. Efficiency roll-off in organic light-emitting diodes. *Adv. Mater.* **25**, 6801–6827 (2013).
27. Chiu, C.-H. et al. A phosphorescent OLED with an efficiency roll-off lower than 1% at 10000 cd m⁻² achieved by reducing the carrier mobility of the donors in an exciplex co-host system. *J. Mater. Chem. C* **10**, 4955–4964 (2022).
28. Giebink, N. C. & Forrest, S. R. Quantum efficiency roll-off at high brightness in fluorescent and phosphorescent organic light emitting diodes. *Phys. Rev. B* **77**, 235215 (2008).
29. Huang, Y., Hsiang, E. L., Deng, M. Y. & Wu, S. T. Mini-LED, Micro-LED and OLED displays: present status and future perspectives. *Light: Sci. Appl.* **9**, 105 (2020).
30. Lighthart, A. et al. Effect of triplet confinement on triplet-triplet annihilation in organic phosphorescent host-guest systems. *Adv. Funct. Mater.* **28**, 1804618 (2018).
31. Coehoorn, R., van Eersel, H., Bobbert, P. A. & Janssen, R. A. J. Kinetic Monte Carlo study of the sensitivity of OLED efficiency and lifetime to materials parameters. *Adv. Funct. Mater.* **25**, 2024–2037 (2015).
32. Masui, K., Nakanotani, H. & Adachi, C. Analysis of exciton annihilation in high-efficiency sky-blue organic light-emitting diodes with thermally activated delayed fluorescence. *Org. Electron.* **14**, 2721–2726 (2013).
33. Hasan, M. et al. Probing polaron-induced exciton quenching in TADF based organic light-emitting diodes. *Nat. Commun.* **13**, 254 (2022).
34. Thakur, K., Zee, B., Wetzelaer, G. J. A. H., Ramanan, C. & Blom, P. W. M. Quantifying exciton annihilation effects in thermally activated delayed fluorescence materials. *Adv. Opt. Mater.* **10**, 2101784 (2021).
35. Scholz, S., Kondakov, D., Lussem, B. & Leo, K. Degradation mechanisms and reactions in organic light-emitting devices. *Chem. Rev.* **115**, 8449–8503 (2015).
36. Dias, F. B., Penfold, T. J. & Monkman, A. P. Photophysics of thermally activated delayed fluorescence molecules. *Methods. Appl. Fluoresc.* **5**, 012001 (2017).
37. Tsuchiya, Y. et al. Exact solution of kinetic analysis for thermally activated delayed fluorescence materials. *J. Phys. Chem. A* **125**, 8074–8089 (2021).
38. Matsuo, K. & Yasuda, T. Blue thermally activated delayed fluorescence emitters incorporating acridan analogues with heavy group 14 elements for high-efficiency doped and non-doped OLEDs. *Chem. Sci.* **10**, 10687–10697 (2019).
39. Kim, J. U. et al. Nanosecond-time-scale delayed fluorescence molecule for deep-blue OLEDs with small efficiency rolloff. *Nat. Commun.* **11**, 1765 (2020).
40. Wong, M. Y. et al. Deep-blue oxadiazole-containing thermally activated delayed fluorescence emitters for organic light-emitting diodes. *ACS Appl. Mater. Interfaces* **10**, 33360–33372 (2018).
41. Serevičius, T. et al. TADF parameters in the solid state: an easy way to draw wrong conclusions. *J. Phys. Chem. A* **125**, 1637–1641 (2021).
42. Niwa, A. et al. Triplet-triplet annihilation in a thermally activated delayed fluorescence emitter lightly doped in a host. *Appl. Phys. Lett.* **113**, 083301 (2018).
43. Rossi, D., Palazzo, D., Di Carlo, A. & Auf der Maur, M. Drift-diffusion study of the IQE roll-off in blue thermally activated delayed fluorescence OLEDs. *Adv. Electron. Mater.* **6**, 2000245 (2020).
44. Serevičius, T. et al. Emission wavelength dependence on the rISC rate in TADF compounds with large conformational disorder. *Chem. Commun.* **55**, 1975–1978 (2019).
45. Kelly, D., Franca, L. G., Stavrou, K., Danos, A. & Monkman, A. P. Laplace transform fitting as a tool to uncover distributions of reverse intersystem crossing rates in TADF systems. *J. Phys. Chem. Lett.* **13**, 6981–6986 (2022).
46. BT.2020: Parameter Values for Ultra-High Definition Television Systems for Production and International Programme Exchange. *ITN www.itu.int/rec/R-REC-BT.2020-2-201510-l/en* (2015).
47. Nakanotani, H. et al. High-efficiency organic light-emitting diodes with fluorescent emitters. *Nat. Commun.* **5**, 5016 (2014).
48. Duan, C. et al. Multi-dipolar chromophores featuring phosphine oxide as joint acceptor: a new strategy toward high-efficiency blue thermally activated delayed fluorescence dyes. *Chem. Mat.* **28**, 5667–5679 (2016).
49. Yang, T. et al. Improving the efficiency of red thermally activated delayed fluorescence organic light-emitting diode by rational isomer engineering. *Adv. Funct. Mater.* **30**, 2002681 (2020).
50. Park, I. S., Lee, J. & Yasuda, T. High-performance blue organic light-emitting diodes with 20% external electroluminescence quantum efficiency based on pyrimidine-containing thermally activated delayed fluorescence emitters. *J. Mater. Chem. C* **4**, 7911–7916 (2016).
51. Zhang, D., Cai, M., Zhang, Y., Zhang, D. & Duan, L. Sterically shielded blue thermally activated delayed fluorescence emitters with improved efficiency and stability. *Mater. Horiz.* **3**, 145–151 (2016).
52. Lee, J., Aizawa, N. & Yasuda, T. Isobenzofuranone- and chromone-based blue delayed fluorescence emitters with low efficiency roll-off in organic light-emitting diodes. *Chem. Mat.* **29**, 8012–8020 (2017).
53. Miwa, T. et al. Blue organic light-emitting diodes realizing external quantum efficiency over 25% using thermally activated delayed fluorescence emitters. *Sci. Rep.* **7**, 284 (2017).
54. Park, I. S., Komiya, H. & Yasuda, T. Pyrimidine-based twisted donor-acceptor delayed fluorescence molecules: a new universal platform for highly efficient blue electroluminescence. *Chem. Sci.* **8**, 953–960 (2017).
55. Rajamalli, P. et al. New molecular design concurrently providing superior pure blue, thermally activated delayed fluorescence and optical out-coupling efficiencies. *J. Am. Chem. Soc.* **139**, 10948–10951 (2017).
56. Chen, J. X. et al. Red organic light-emitting diode with external quantum efficiency beyond 20% based on a novel thermally activated delayed fluorescence emitter. *Adv. Sci.* **5**, 1800436 (2018).
57. Furue, R. et al. Highly efficient red-orange delayed fluorescence emitters based on strong π -accepting dibenzophenazine and dibenzoquinoxaline cores: toward a rational pure-red OLED design. *Adv. Opt. Mater.* **6**, 1701147 (2018).
58. Zhang, D., Song, X., Cai, M., Kaji, H. & Duan, L. Versatile indolocarbazole-isomer derivatives as highly emissive emitters and ideal hosts for thermally activated delayed fluorescent OLEDs with alleviated efficiency roll-off. *Adv. Mater.* **30**, 1705406 (2018).
59. Ahn, D. H. et al. Highly twisted donor-acceptor boron emitter and high triplet host material for highly efficient blue thermally activated delayed fluorescent device. *ACS Appl. Mater. Interfaces* **11**, 14909–14916 (2019).
60. Braveenth, R. et al. High efficiency green TADF emitters of acridine donor and triazine acceptor D–A–D structures. *J. Mater. Chem. C* **7**, 7672–7680 (2019).
61. Chen, J. X. et al. Red/near-infrared thermally activated delayed fluorescence OLEDs with near 100% internal quantum efficiency. *Angew. Chem. Int. Ed.* **58**, 14660–14665 (2019).
62. Cheng, Z. et al. Achieving efficient blue delayed electrofluorescence by shielding acceptors with carbazole units. *ACS Appl. Mater. Interfaces* **11**, 28096–28105 (2019).
63. Xie, F. M. et al. Rational molecular design of dibenzo[a,c]phenazine-based thermally activated delayed fluorescence emitters for orange-red OLEDs with EQE up to 22.0. *ACS Appl. Mater. Interfaces* **11**, 26144–26151 (2019).
64. Xie, F. M. et al. Efficient orange-red delayed fluorescence organic light-emitting diodes with external quantum efficiency over 26%. *Adv. Electron. Mater.* **6**, 1900843 (2019).
65. Balijapalli, U. et al. Utilization of multi-heterodonor in thermally activated delayed fluorescence molecules and their high performance bluish-green organic light-emitting diodes. *ACS Appl. Mater. Interfaces* **12**, 9498–9506 (2020).
66. Kumar, A. et al. Doubly boron-doped TADF emitters decorated with ortho-donor groups for highly efficient green to red OLEDs. *Chem. Eur. J.* **26**, 16793–16801 (2020).
67. Lim, H. et al. Highly efficient deep-blue OLEDs using a TADF emitter with a narrow emission spectrum and high horizontal emitting dipole ratio. *Adv. Mater.* **32**, e2004083 (2020).
68. Peng, C. C. et al. Highly efficient thermally activated delayed fluorescence via an unconjugated donor-acceptor system realizing EQE of over 30. *Adv. Mater.* **32**, e2003885 (2020).
69. Yoon, J. et al. Asymmetric host molecule bearing pyridine core for highly efficient blue thermally activated delayed fluorescence OLEDs. *Chem. Eur. J.* **26**, 16383–16391 (2020).
70. Balijapalli, U. et al. Tetrabenzo[a,c]phenazine backbone for highly efficient orange-red thermally activated delayed fluorescence with completely horizontal molecular orientation. *Angew. Chem. Int. Ed.* **60**, 19364–19373 (2021).
71. Chan, C.-Y. et al. Stable pure-blue hyperfluorescence organic light-emitting diodes with high-efficiency and narrow emission. *Nat. Photonics* **15**, 203–207 (2021).
72. Chen, J. X. et al. Managing locally excited and charge-transfer triplet states to facilitate up-conversion in red TADF emitters that are available for both vacuum- and solution-processes. *Angew. Chem. Int. Ed.* **60**, 2478–2484 (2021).
73. Chen, Y. et al. Approaching nearly 40% external quantum efficiency in organic light emitting diodes utilizing a green thermally activated delayed fluorescence emitter with an extended linear donor-acceptor-donor structure. *Adv. Mater.* **33**, e2103293 (2021).
74. Duan, C. et al. Manipulating charge-transfer excitons by exciplex matrix: toward thermally activated delayed fluorescence diodes with power efficiency beyond 110 lm W⁻¹. *Adv. Funct. Mater.* **31**, 2102739 (2021).
75. Karthik, D. et al. Acceptor-donor-acceptor-type orange-red thermally activated delayed fluorescence materials realizing external quantum efficiency over 30% with low efficiency roll-off. *Adv. Mater.* **33**, e2007724 (2021).
76. Kim, H., Lee, Y., Lee, H., Hong, J. I. & Lee, D. Click-to-twist strategy to build blue-to-green emitters: bulky triazoles for electronically tunable and thermally activated delayed fluorescence. *ACS Appl. Mater. Interfaces* **13**, 12286–12295 (2021).
77. Nagata, M. et al. Fused-nonacyclic multi-resonance delayed fluorescence emitter based on ladder-thiaborin exhibiting narrowband sky-blue emission with accelerated reverse intersystem crossing. *Angew. Chem. Int. Ed.* **60**, 20280–20285 (2021).
78. Tanaka, H. et al. Hypsochromic shift of multiple-resonance-induced thermally activated delayed fluorescence by oxygen atom incorporation. *Angew. Chem. Int. Ed.* **60**, 17910–17914 (2021).
79. Chen, J. X. et al. Optimizing intermolecular interactions and energy level alignments of red TADF emitters for high-performance organic light-emitting diodes. *Small* **18**, e2201548 (2022).
80. Gao, H. et al. Ultrapure blue thermally activated delayed fluorescence (TADF) emitters based on rigid sulfur/oxygen-bridged triarylboron acceptor: MR TADF and D-A TADF. *J. Phys. Chem. Lett.* **13**, 7561–7567 (2022).
81. Mahmoudi, M. et al. Ornameting of blue thermally activated delayed fluorescence emitters by anchor groups for the minimization of solid-state solvation and conformation disorder corollaries in non-doped and doped organic light-emitting diodes. *ACS Appl. Mater. Interfaces* **14**, 40158–40172 (2022).

82. Mamada, M. et al. Highly efficient deep-blue organic light-emitting diodes based on rational molecular design and device engineering. *Adv. Funct. Mater.* **32**, 2204352 (2022).
83. Masimukku, N. et al. Bipolar 1,8-naphthalimides showing high electron mobility and red AIE-active TADF for OLED applications. *Phys. Chem. Chem. Phys.* **24**, 5070–5082 (2022).
84. Zhang, H. Y. et al. A novel orange-red thermally activated delayed fluorescence emitter with high molecular rigidity and planarity realizing 32.5% external quantum efficiency in organic light-emitting diodes. *Mater. Horiz.* **9**, 2425–2432 (2022).
85. Xia, G. et al. A TADF emitter featuring linearly arranged spiro-donor and spiro-acceptor groups: efficient nondoped and doped deep-blue OLEDs with CIE(y) <0.1. *Angew. Chem. Int. Ed.* **60**, 9598–9603 (2021).
86. Song, W. et al. [1,2,4]Triazolo[1,5-a]pyridine-based host materials for green phosphorescent and delayed-fluorescence OLEDs with low efficiency roll-off. *ACS Appl. Mater. Interfaces* **10**, 24689–24698 (2018).
87. Li, W., Li, J., Liu, D., Wang, F. & Zhang, S. Bipolar host materials for high-efficiency blue phosphorescent and delayed-fluorescence OLEDs. *J. Mater. Chem. C* **3**, 12529–12538 (2015).
88. Zhang, Z. et al. Excited-state engineering of universal ambipolar hosts for highly efficient blue phosphorescence and thermally activated delayed fluorescence organic light-emitting diodes. *Chem. Eng. J.* **382**, 122485 (2020).
89. Ni, F. et al. Teaching an old acceptor new tricks: rationally employing 2,1,3-benzothiazazole as input to design a highly efficient red thermally activated delayed fluorescence emitter. *J. Mater. Chem. C* **5**, 1363–1368 (2017).
90. Zhang, Y. L. et al. High-efficiency red organic light-emitting diodes with external quantum efficiency close to 30% based on a novel thermally activated delayed fluorescence emitter. *Adv. Mater.* **31**, e1902368 (2019).
91. Gong, X. et al. A red thermally activated delayed fluorescence emitter simultaneously having high photoluminescence quantum efficiency and preferentially horizontal emitting dipole orientation. *Adv. Funct. Mater.* **30**, 1908839 (2020).
92. Wang, Y. Y. et al. Positive impact of chromophore flexibility on the efficiency of red thermally activated delayed fluorescence materials. *Mater. Horiz.* **8**, 1297–1303 (2021).
93. Kim, B. S. & Lee, J. Y. Engineering of mixed host for high external quantum efficiency above 25% in green thermally activated delayed fluorescence device. *Adv. Funct. Mater.* **24**, 3970–3977 (2014).
94. Sun, J. W. et al. A fluorescent organic light-emitting diode with 30% external quantum efficiency. *Adv. Mater.* **26**, 5684–5688 (2014).
95. Seino, Y., Inomata, S., Sasabe, H., Pu, Y. J. & Kido, J. High-performance green OLEDs using thermally activated delayed fluorescence with a power efficiency of over 100 lmW⁻¹. *Adv. Mater.* **28**, 2638–2643 (2016).
96. Sasabe, H. et al. Ultrahigh power efficiency thermally activated delayed fluorescent OLEDs by the strategic use of electron-transport materials. *Adv. Opt. Mater.* **6**, 1800376 (2018).
97. Zhang, X. et al. Host-free yellow-green organic light-emitting diodes with external quantum efficiency over 20% based on a compound exhibiting thermally activated delayed fluorescence. *ACS Appl. Mater. Interfaces* **11**, 12693–12698 (2019).
98. Liu, H. et al. Modulating the acceptor structure of dicyanopyridine based TADF emitters: Nearly 30% external quantum efficiency and suppression on efficiency roll-off in OLED. *Chem. Eng. J.* **401**, 126107 (2020).
99. Chen, C.-H. et al. New bipolar host materials for high power efficiency green thermally activated delayed fluorescence OLEDs. *Chem. Eng. J.* **442**, 136292 (2022).
100. Zhang, Q. et al. Efficient blue organic light-emitting diodes employing thermally activated delayed fluorescence. *Nat. Photonics* **8**, 326–332 (2014).
101. Hirata, S. et al. Highly efficient blue electroluminescence based on thermally activated delayed fluorescence. *Nat. Mater.* **14**, 330–336 (2015).
102. Sun, J. W. et al. Thermally activated delayed fluorescence from azasilane based intramolecular charge-transfer emitter (DTPDDA) and a highly efficient blue light emitting diode. *Chem. Mater.* **27**, 6675–6681 (2015).
103. Komatsu, R., Sasabe, H., Seino, Y., Nakao, K. & Kido, J. Light-blue thermally activated delayed fluorescent emitters realizing a high external quantum efficiency of 25% and unprecedented low drive voltages in OLEDs. *J. Mater. Chem. C* **4**, 2274–2278 (2016).
104. Lee, I. & Lee, J. Y. Molecular design of deep blue fluorescent emitters with 20% external quantum efficiency and narrow emission spectrum. *Org. Electron.* **29**, 160–164 (2016).
105. Lee, S. Y., Adachi, C. & Yasuda, T. High-efficiency blue organic light-emitting diodes based on thermally activated delayed fluorescence from phenoxaphosphine and phenoxathiin derivatives. *Adv. Mater.* **28**, 4626–4631 (2016).
106. Lin, T. A. et al. Sky-blue organic light emitting diode with 37% external quantum efficiency using thermally activated delayed fluorescence from spiroacridine-triazine hybrid. *Adv. Mater.* **28**, 6976–6983 (2016).
107. Rajamalli, P. et al. A method for reducing the singlet-triplet energy gaps of TADF materials for improving the blue OLED efficiency. *ACS Appl. Mater. Interfaces* **8**, 27026–27034 (2016).
108. Sun, J. W., Kim, K. H., Moon, C. K., Lee, J. H. & Kim, J. J. Highly efficient sky-blue fluorescent organic light emitting diode based on mixed cohost system for thermally activated delayed fluorescence emitter (2CzPn). *ACS Appl. Mater. Interfaces* **8**, 9806–9810 (2016).
109. Rajamalli, P. et al. Thermally activated delayed fluorescence emitters with a m,m-di-tert-butyl-carbazolyl benzoylpyridine core achieving extremely high blue electroluminescence efficiencies. *J. Mater. Chem. C* **5**, 2919–2926 (2017).
110. Xu, Y. et al. Highly efficient blue fluorescent OLEDs based on upper level triplet-singlet intersystem crossing. *Adv. Mater.* **31**, e1807388 (2019).
111. Bian, J. et al. Ambipolar self-host functionalization accelerates blue multi-resonance thermally activated delayed fluorescence with internal quantum efficiency of 100. *Adv. Mater.* **34**, e2110547 (2022).
112. Cheon, H. J., Woo, S. J., Baek, S. H., Lee, J. H. & Kim, Y. H. Dense local triplet states and steric shielding of a multi-resonance TADF emitter enable high-performance deep-blue OLEDs. *Adv. Mater.* **34**, e2207416 (2022).
113. Mei, Y., Liu, D., Li, J. & Wang, J. Accelerating PLQY and RISC rates in deep-blue TADF materials with the acridin-9(10H)-one acceptor by tuning the peripheral groups on carbazole donors. *J. Mater. Chem. C* **10**, 16524–16535 (2022).
114. Matsushima, T. & Adachi, C. Enhanced hole injection and transport in molybdenum-dioxide-doped organic hole-transporting layers. *J. Appl. Phys.* **103**, 034501 (2008).
115. Kim, K.-H., Moon, C.-K., Sun, J. W., Sim, B. & Kim, J.-J. Triplet harvesting by a conventional fluorescent emitter using reverse intersystem crossing of host triplet exciplex. *Adv. Opt. Mater.* **3**, 895–899 (2015).
116. Zhao, B. et al. Highly efficient red OLEDs using DCJTb as the dopant and delayed fluorescent exciplex as the host. *Sci. Rep.* **5**, 10697 (2015).
117. Hung, W. Y. et al. Balance the carrier mobility to achieve high performance exciplex OLED using a triazine-based acceptor. *ACS Appl. Mater. Interfaces* **8**, 4811–4818 (2016).
118. Lo, Y. C. et al. High-efficiency red and near-infrared organic light-emitting diodes enabled by pure organic fluorescent emitters and an exciplex-forming cohost. *ACS Appl. Mater. Interfaces* **11**, 23417–23427 (2019).
119. Xia, G. et al. Organoboron compounds constructed through the tautomerization of 1H-indole to 3H-indole for red OLEDs. *J. Mater. Chem. C* **9**, 6834–6840 (2021).
120. Bang, H.-S., Yun, J. & Lee, C. Improved lifetime and efficiency of green organic light-emitting diodes with a fluorescent dye (C545T)-doped hole transport layer. In *Proc. SPIE, Organic Light Emitting Materials and Devices XI* (eds Kafafi, Z. H. & So, F.) 66551W–1–66551W-7 (SPIE, 2007).
121. Benor, A., Takizawa, S.-y., Pérez-Bolívar, C. & Anzenbacher, P. Efficiency improvement of fluorescent OLEDs by tuning the working function of PEDOT:PSS using UV-ozone exposure. *Org. Electron.* **11**, 938–945 (2010).
122. Liu, X. K. et al. Nearly 100% triplet harvesting in conventional fluorescent dopant-based organic light-emitting devices through energy transfer from exciplex. *Adv. Mater.* **27**, 2025–2030 (2015).
123. Jang, H. J. & Lee, J. Y. Suppressed nonradiative decay of an exciplex by an inert host for efficiency improvement in a green fluorescence organic light-emitting diode. *J. Phys. Chem. C* **123**, 26856–26861 (2019).
124. Liang, B., Wang, J., Cheng, Z., Wei, J. & Wang, Y. Exciplex-based electroluminescence: over 21% external quantum efficiency and approaching 100 lm/W power efficiency. *J. Phys. Chem. Lett.* **10**, 2811–2816 (2019).
125. Zheng, C.-J. et al. Highly efficient non-doped deep-blue organic light-emitting diodes based on anthracene derivatives. *J. Mater. Chem.* **20**, 1560–1566 (2010).
126. Sych, G. et al. Exciplex-enhanced singlet emission efficiency of nondoped organic light emitting diodes based on derivatives of tetrafluorophenylcarbazole and tri/tetraphenylethylene exhibiting aggregation-induced emission enhancement. *J. Phys. Chem. C* **122**, 14827–14837 (2018).
127. Tasaki, S. et al. Realization of ultra-high-efficient fluorescent blue OLED. *J. Soc. Inf. Disp.* **30**, 441–451 (2022).
128. Zhao, J. et al. Highly efficient green and red OLEDs based on a new exciplex system with simple structures. *Org. Electron.* **43**, 136–141 (2017).
129. Shih, C. J. et al. Versatile exciplex-forming co-host for improving efficiency and lifetime of fluorescent and phosphorescent organic light-emitting diodes. *ACS Appl. Mater. Interfaces* **10**, 24090–24098 (2018).
130. Reineke, S., Walzer, K. & Leo, K. Triplet-exciton quenching in organic phosphorescent light-emitting diodes with Ir-based emitters. *Phys. Rev. B* **75**, 125328 (2007).
131. Fukagawa, H. et al. Highly efficient and stable red phosphorescent organic light-emitting diodes using platinum complexes. *Adv. Mater.* **24**, 5099–5103 (2012).
132. Kwak, J. et al. New carbazole-based host material for low-voltage and highly efficient red phosphorescent organic light-emitting diodes. *J. Mater. Chem.* **22**, 6351–6355 (2012).
133. Chen, C.-H. et al. Highly efficient orange and deep-red organic light emitting diodes with long operational lifetimes using carbazole–quinoline based bipolar host materials. *J. Mater. Chem. C* **2**, 6183–6191 (2014).
134. Lee, J. H., Shin, H., Kim, J. M., Kim, K. H. & Kim, J. J. Exciplex-forming co-host-based red phosphorescent organic light-emitting diodes with long operational stability and high efficiency. *ACS Appl. Mater. Interfaces* **9**, 3277–3281 (2017).
135. Jia, L. et al. High-performance exciplex-type host for multicolor phosphorescent organic light-emitting diodes with low turn-on voltages. *ACS Sustain. Chem. Eng.* **6**, 8809–8815 (2018).
136. Liu, X.-Y. et al. 9-Silafluorene and 9-germafluorene: novel platforms for highly efficient red phosphorescent organic light-emitting diodes. *J. Mater. Chem. C* **6**, 8144–8151 (2018).
137. Wang, Y. et al. High-efficiency red organic light-emitting diodes based on a double-emissive layer with an external quantum efficiency over 30%. *J. Mater. Chem. C* **6**, 7042–7045 (2018).
138. Ito, T. et al. A series of dibenzofuran-based n-type exciplex host partners realizing high-efficiency and stable deep-red phosphorescent OLEDs. *Chem. Eur. J.* **25**, 7308–7314 (2019).
139. Tian, Q. S. et al. Multichannel effect of triplet excitons for highly efficient green and red phosphorescent OLEDs. *Adv. Opt. Mater.* **8**, 2000556 (2020).
140. Kim, S.-Y. et al. Organic light-emitting diodes with 30% external quantum efficiency based on a horizontally oriented emitter. *Adv. Funct. Mater.* **23**, 3896–3900 (2013).
141. Li, G. et al. Very high efficiency orange-red light-emitting devices with low roll-off at high luminance based on an ideal host-guest system consisting of two novel phosphorescent iridium complexes with bipolar transport. *Adv. Funct. Mater.* **24**, 7420–7426 (2014).
142. Liu, J. et al. Achieving above 30% external quantum efficiency for inverted phosphorescence organic light-emitting diodes based on ultrathin emitting layer. *Org. Electron.* **15**, 2492–2498 (2014).
143. Seo, S. et al. Exciplex-triplet energy transfer: a new method to achieve extremely efficient organic light-emitting diode with external quantum efficiency over 30% and drive voltage below 3 V. *Jpn J. Appl. Phys.* **53**, 042102 (2014).
144. Shih, C. J. et al. Exciplex-forming cohost for high efficiency and high stability phosphorescent organic light-emitting diodes. *ACS Appl. Mater. Interfaces* **10**, 2151–2157 (2018).
145. Tsai, M. H. et al. 3-(9-Carbazolyl)carbazoles and 3,6-di(9-carbazolyl)carbazoles as effective host materials for efficient blue organic electrophosphorescence. *Adv. Mater.* **19**, 862–866 (2007).

146. Su, S.-J., Takahashi, Y., Chiba, T., Takeda, T. & Kido, J. Structure-property relationship of pyridine-containing triphenyl benzene electron-transport materials for highly efficient blue phosphorescent OLEDs. *Adv. Funct. Mater.* **19**, 1260–1267 (2009).
147. Lee, J., Lee, J.-I., Lee, J.-W. & Chu, H. Y. Effects of charge balance on device performances in deep blue phosphorescent organic light-emitting diodes. *Org. Electron.* **11**, 1159–1164 (2010).
148. Jeon, S. O., Jang, S. E., Son, H. S. & Lee, J. Y. External quantum efficiency above 20% in deep blue phosphorescent organic light-emitting diodes. *Adv. Mater.* **23**, 1436–1441 (2011).
149. Lee, C. W. & Lee, J. Y. Above 30% external quantum efficiency in blue phosphorescent organic light-emitting diodes using pyrido[2,3-b]indole derivatives as host materials. *Adv. Mater.* **25**, 5450–5454 (2013).
150. Fleetham, T., Li, G., Wen, L. & Li, J. Efficient 'pure' blue OLEDs employing tetradentate Pt complexes with a narrow spectral bandwidth. *Adv. Mater.* **26**, 7116–7121 (2014).
151. Udagawa, K., Sasabe, H., Cai, C. & Kido, J. Low-driving-voltage blue phosphorescent organic light-emitting devices with external quantum efficiency of 30%. *Adv. Mater.* **26**, 5062–5066 (2014).
152. Lee, J.-H. et al. An exciplex forming host for highly efficient blue organic light emitting diodes with low driving voltage. *Adv. Funct. Mater.* **25**, 361–366 (2015).
153. Lim, H. et al. An exciplex host for deep-blue phosphorescent organic light-emitting diodes. *ACS Appl. Mater. Interfaces* **9**, 37883–37887 (2017).
154. Wang, Z. et al. Manipulation of thermally activated delayed fluorescence of blue exciplex emission: fully utilizing exciton energy for highly efficient organic light emitting diodes with low roll-off. *ACS Appl. Mater. Interfaces* **9**, 21346–21354 (2017).
155. Idris, M. et al. Blue emissive fac/mer-iridium (III) NHC carbene complexes and their application in OLEDs. *Adv. Opt. Mater.* **9**, 2001994 (2021).

Publisher's note Springer Nature remains neutral with regard to jurisdictional claims in published maps and institutional affiliations.



Open Access This article is licensed under a Creative Commons Attribution 4.0 International License, which permits use, sharing, adaptation, distribution and reproduction in any medium or format, as long as you give appropriate credit to the original author(s) and the source, provide a link to the Creative Commons licence, and indicate if changes were made. The images or other third party material in this article are included in the article's Creative Commons licence, unless indicated otherwise in a credit line to the material. If material is not included in the article's Creative Commons licence and your intended use is not permitted by statutory regulation or exceeds the permitted use, you will need to obtain permission directly from the copyright holder. To view a copy of this licence, visit <http://creativecommons.org/licenses/by/4.0/>.

© The Author(s) 2024

Analysis

Methods

Data collection

We considered the reported efficiency roll-off behaviour of TADF OLEDs published in peer-reviewed journals between 2016 and 2022. The data of the OLED and emitter were included in the analysis if the following criteria were met:

1. The reported OLED was vacuum-processed, in a bottom-emitting device structure with a TADF emitter in a host material.
2. Photophysical characterization of the thin film used as the emission layer was reported.
3. The photoluminescence quantum of the emitter film was reported to exceed 60%.
4. The calculation of all TADF rate constants was clearly detailed.
5. Device data clearly showed J_{90} data or the presented device data allowed for a reasonable estimation of J_{90} .

Applying these criteria led to a total of 66 devices from 46 publications being included in our analysis^{5,38,39,48–84,156–160}.

For comparison, Fig. 1c shows the relation between J_{90} and the EQE at 1,000 cd m⁻² (EQE_{1,000}) for TADF OLEDs^{5,38,39,48–113} with representative fluorescent^{28,114–129} and phosphorescent^{86–88,128–155} devices across red, green and blue colours.

Steady-state population of the excited states

The kinetics of a TADF emitter as shown in Fig. 2 under electrical excitation can be described by the rate equations for the excited singlet state (S_1) and the triplet state (T_1) when neglecting annihilation processes as follows.

$$\frac{d}{dt}[S_1]_t = - \underbrace{(k_r^S + k_{nr}^S + k_{ISC})}_{=k^S} [S_1]_t + k_{RISC}[T_1]_t + \frac{1}{4}\gamma[n]_t^2 \quad (5)$$

$$\frac{d}{dt}[T_1]_t = - \underbrace{(k_r^T + k_{nr}^T + k_{RISC})}_{=k^T} [T_1]_t + k_{ISC}[S_1]_t + \frac{3}{4}\gamma[n]_t^2 \quad (6)$$

where k^S is the sum of the rate constants for ISC (k_{ISC}), radiative (k_r^S) and non-radiative (k_{nr}^S) decay from S_1 , where k^T is the sum of the rate constants for RISC (k_{RISC}), radiative (k_r^T) and non-radiative (k_{nr}^T) decay from T_1 , and γ is the Langevin recombination rate. The derivative of the polaron population $[n]_t$ can be sufficiently approximated by not distinguishing between the charge of the polaron as

$$\frac{d}{dt}[n]_t = \frac{J(t)}{ed} - \gamma[n]_t^2, \quad (7)$$

where $J(t)$ is the current density at time t , d is the thickness of the emission zone and e is the elementary charge.

In normal device operation, the OLED is driven at constant current density ($J(t) = J_{const}$) so the excited-state populations reach a steady state given by equation (8).

$$[n] = \sqrt{\frac{J_{const}}{\gamma ed}}. \quad (8)$$

The steady-state population of S_1 and T_1 ($[S_1]$ and $[T_1]$, respectively) can be obtained by substituting the differential equation for S_1 in steady state into the differential equation of T_1 steady state

$$\frac{d}{dt}[S_1] = -k^S[S_1] + k_{RISC}[T_1] + \frac{1}{4}\gamma[n]^2 = 0 \quad (9)$$

$$\Rightarrow [S_1] = \frac{k_{RISC}[T_1] + \frac{1}{4}\gamma[n]^2}{k^S} \quad (10)$$

$$\frac{d}{dt}[T_1] = -k^T[T_1] + k_{ISC}[S_1] + \frac{3}{4}\gamma[n]^2 = 0 \quad (11)$$

$$\Rightarrow [T_1] = \frac{k_{ISC} \frac{k_{RISC}[T_1] + \frac{1}{4}\gamma[n]^2}{k^S} + \frac{3}{4}\gamma[n]^2}{k^T} = \frac{k_{ISC}k_{RISC}[T_1] + \left(\frac{k_{ISC}}{k^S} + 3\right)\frac{\gamma[n]^2}{4k^T}}{k^S k^T} \quad (12)$$

$$\Leftrightarrow [T_1] = \frac{\left(\frac{k_{ISC}}{k^S} + 3\right)\frac{\gamma[n]^2}{4k^T}}{1 - \frac{k_{ISC}k_{RISC}}{k^S k^T}} = \frac{k_{ISC} + 3k^S}{4(k^T k^S - k_{ISC}k_{RISC})} \gamma[n]^2 \quad (13)$$

$$= \frac{3k_r^S + 3k_{nr}^S + 4k_{ISC}}{4k^S(k_r^T + k_{nr}^T) + 4k_{RISC}(k_r^S + k_{nr}^S)} \gamma[n]^2$$

$$\Rightarrow [S_1] = \frac{1}{k^S} \left(k_{RISC}[T_1] + \frac{1}{4}\gamma[n]^2 \right) = \left(k_{RISC} \frac{k_{ISC} + 3k^S}{(k^T k^S - k_{ISC}k_{RISC})} + 1 \right) \frac{\gamma[n]^2}{4k^S} \quad (14)$$

$$= \left(k_{RISC} \frac{k_{ISC} + 3k^S}{k^S(k_r^T + k_{nr}^T) + k_{RISC}(k_r^S + k_{nr}^S)} + 1 \right) \frac{\gamma[n]^2}{4k^S}$$

By inserting equation (8) in equations (13) and (14) the steady-state populations are given as a function of the current density as

$$[S_1] = \left(k_{RISC} \frac{3k_r^S + 3k_{nr}^S + 4k_{ISC}}{k^S(k_r^T + k_{nr}^T) + k_{RISC}(k_r^S + k_{nr}^S)} + 1 \right) \frac{1}{4k^S} \frac{J_{const}}{ed} \quad (15)$$

$$[T_1] = \frac{3k_r^S + 3k_{nr}^S + 4k_{ISC}}{4k^S(k_r^T + k_{nr}^T) + 4k_{RISC}(k_r^S + k_{nr}^S)} \frac{J_{const}}{ed} \quad (16)$$

Calculation of J_{90} for OLED examples

A set of 1,287 kinetic parameters for the equations (5) and (6) was generated, using the permutation of the input variables in Extended Data Table 1, with

$$k_{RISC} = k_r^S K_{eq} \left(\frac{3}{4} + \frac{k_{ISC}}{k_r^S} \right) \quad (17)$$

and a thickness of the emission zone of $d = 10$ nm, a Langevin recombination rate¹⁶¹ of $\gamma = 6.8 \times 10^{-17} \frac{m^3}{s}$ as well as all other rate constants set to 0.

For the calculation of Extended Data Fig. 3a,b, the bimolecular rate constants were set to the values shown in the figure. J_{90} was obtained by minimizing equation (18) using the python package `scipy`¹⁶².

$$(\bar{\eta}_{EQE} - 0.9)^2 = \left(\frac{\eta_{EQE}(J)}{\eta_{EQE}^0} - 0.9 \right)^2 = \left(\frac{\eta_{IQE}(J)}{\eta_{IQE}^0} - 0.9 \right)^2 \quad (18)$$

where $\eta_{IQE}(J)$ is the internal quantum efficiency (IQE) at current density J considering annihilation processes and η_{IQE}^0 is the IQE without considering annihilation processes. Both are given by

$$\eta_{IQE} = (k_r^S[S_1] + k_r^T[T_1]) \frac{\gamma d}{J} \quad (19)$$

For η_{IQE}^0 the singlet population $[S_1]$ and triplet population $[T_1]$ were obtained from equations (15) and (16), respectively.

For $\eta_{IQE}(J)$, $[S_1]$ and $[T_1]$ were obtained by minimizing the set of differential equations (20) and (21) with $[n]$ given by equation (7), using the python package `scipy`^{161,162}.

$$\frac{d}{dt}[S_1] = - \frac{(k_r^S + k_{nr}^S + k_{ISC})}{=k^S} [S_1] + k_{RISC}[T_1] + \frac{1}{4}\gamma_{TT}[T_1]^2 - \gamma_{ST}[T_1][S_1] + \frac{1}{4}\gamma[n]^2 \quad (20)$$

$$\frac{d}{dt}[T_1] = - \frac{(k_r^T + k_{nr}^T + k_{RISC})}{=k^T} [T_1] + k_{ISC}[S_1] - \frac{5}{4}\gamma_{TT}[T_1]^2 + \frac{3}{4}\gamma[n]^2 \quad (21)$$

Calculation of target value

The optical power flux Φ leaving an OLED relates to the current density J as

$$\Phi_e = \int \Phi_e(\lambda) d\lambda = \int \frac{hc}{\lambda} I(\lambda) \eta_{EQE} \frac{J}{e} d\lambda = \frac{hc}{e} \eta_{EQE} J \int \frac{1}{\lambda} I(\lambda) d\lambda \quad (22)$$

where $I(\lambda)$ is the relative intensity of the OLED at wavelength λ , η_{EQE} is the ratio of photons leaving the OLED to the number of electrons flowing around the electrical circuit (EQE).

The total luminous flux Φ_V can be calculated from the optical power flux using the photonic sensitivity curve $V(\lambda)$ as

$$\Phi_V = K_m \int \Phi_e(\lambda) V(\lambda) d\lambda = K_m \frac{hc}{e} \eta_{EQE} J \int \frac{1}{\lambda} I(\lambda) V(\lambda) d\lambda \quad (23)$$

where $K_m = 683 \text{ lm W}^{-1}$ is a fudge factor called the peak response.

Under the assumption of Lambertian emission, the luminance L_V of the OLED is then given as follows.

$$L_V = \frac{\Phi_V}{\pi} = K_m \frac{hc}{\pi e} \eta_{EQE} J \int \frac{1}{\lambda} I(\lambda) V(\lambda) d\lambda \quad (24)$$

Therefore, the current density required to generate a given luminance by an OLED with a given normalized spectrum and given EQE is given as follows.

$$J = \frac{1}{K_m} \frac{\pi e}{hc} \frac{L_V}{\eta_{EQE}} \left[\int \frac{1}{\lambda} I(\lambda) V(\lambda) d\lambda \right]^{-1} \quad (25)$$

For the calculation of the target value, we have taken three assumed spectra for red, green and blue with a Gaussian shape and a full-width at half-maximum of 45, 30 and 15 nm, respectively. The centre wavelength was selected so that the colours of the three spectra are as close as possible to the primary colours of the BT.2020 standard in the CIE 1931 colour space, which are given by the coordinates (0.708, 0.292), (0.170, 0.797) and (0.131, 0.046), respectively⁴⁶.

The calculation was performed at an EQE of 22.5% for $L_V = 1,000 \text{ cd m}^{-2}$, indicating a maximum EQE of 25%. The correlation for J_{90} to the FOM is

taken from the simulated relationship shown in Extended Data Fig. 4a for $\gamma_{TT} = 10^{-13} \text{ cm}^3 \text{ s}^{-1}$ and $\gamma_{ST} = \gamma_{TP} = 0$ as follows.

$$\log\left(\frac{J_{90}}{1 \text{ Am}^{-2}}\right) = 2 \log\left(\frac{k_r^S K_{eq}}{1 \text{ s}^{-1}}\right) - 8.3764 \quad (26)$$

$$\Leftrightarrow k_r^S K_{eq} = 10^{\frac{\log\left(\frac{J_{90}}{1 \text{ Am}^{-2}}\right) + 8.3764}{2}} \text{ s}^{-1} \quad (27)$$

Data availability

The data supporting this publication can be accessed at <https://doi.org/10.17630/d1439596-7eef-44ae-90cd-667b70588896>.

156. Inoue, M. et al. Effect of reverse intersystem crossing rate to suppress efficiency roll-off in organic light-emitting diodes with thermally activated delayed fluorescence emitters. *Chem. Phys. Lett.* **644**, 62–67 (2016).
157. Yang, M., Park, I. S. & Yasuda, T. Full-color, narrowband, and high-efficiency electroluminescence from boron and carbazole embedded polycyclic heteroaromatics. *J. Am. Chem. Soc.* **142**, 19468–19472 (2020).
158. Oda, S. et al. Carbazole-based DABNA analogues as highly efficient thermally activated delayed fluorescence materials for narrowband organic light-emitting diodes. *Angew. Chem. Int. Ed.* **60**, 2882–2886 (2021).
159. Huang, T., Wang, Q., Meng, G., Duan, L. & Zhang, D. Accelerating radiative decay in blue through-space charge transfer emitters by minimizing the face-to-face donor-acceptor distances. *Angew. Chem. Int. Ed.* **61**, e202200059 (2022).
160. Lv, X. et al. Extending the pi-skeleton of multi-resonance TADF materials towards high-efficiency narrowband deep-blue emission. *Angew. Chem. Int. Ed.* **61**, e202201588 (2022).
161. Grüne, J., Bunzmann, N., Meinecke, M., Dyakonov, V. & Sperlich, A. Kinetic modeling of transient electroluminescence reveals TTA as an efficiency-limiting process in exciplex-based TADF OLEDs. *J. Phys. Chem. C* **124**, 25667–25674 (2020).
162. Virtanen, P. et al. SciPy 1.0: fundamental algorithms for scientific computing in Python. *Nat. Methods* **17**, 261–272 (2020).

Acknowledgements We are grateful to the Engineering and Physical Sciences Research Council of the UK for financial support through grant nos. EP/R035164/1 and EP/P010482/1. We are grateful to K. Yoshida for discussions relating to the target values for the FOM.

Author contributions I.D.W.S. proposed an FOM approach to efficiency roll-off and wrote the first draft of the paper. L.Z. performed the data acquisition. S.D. provided the derivation. L.Z., S.D. and I.D.W.S. performed the analysis. All authors reviewed and edited the manuscript.

Competing interests The authors declare no competing interests.

Additional information

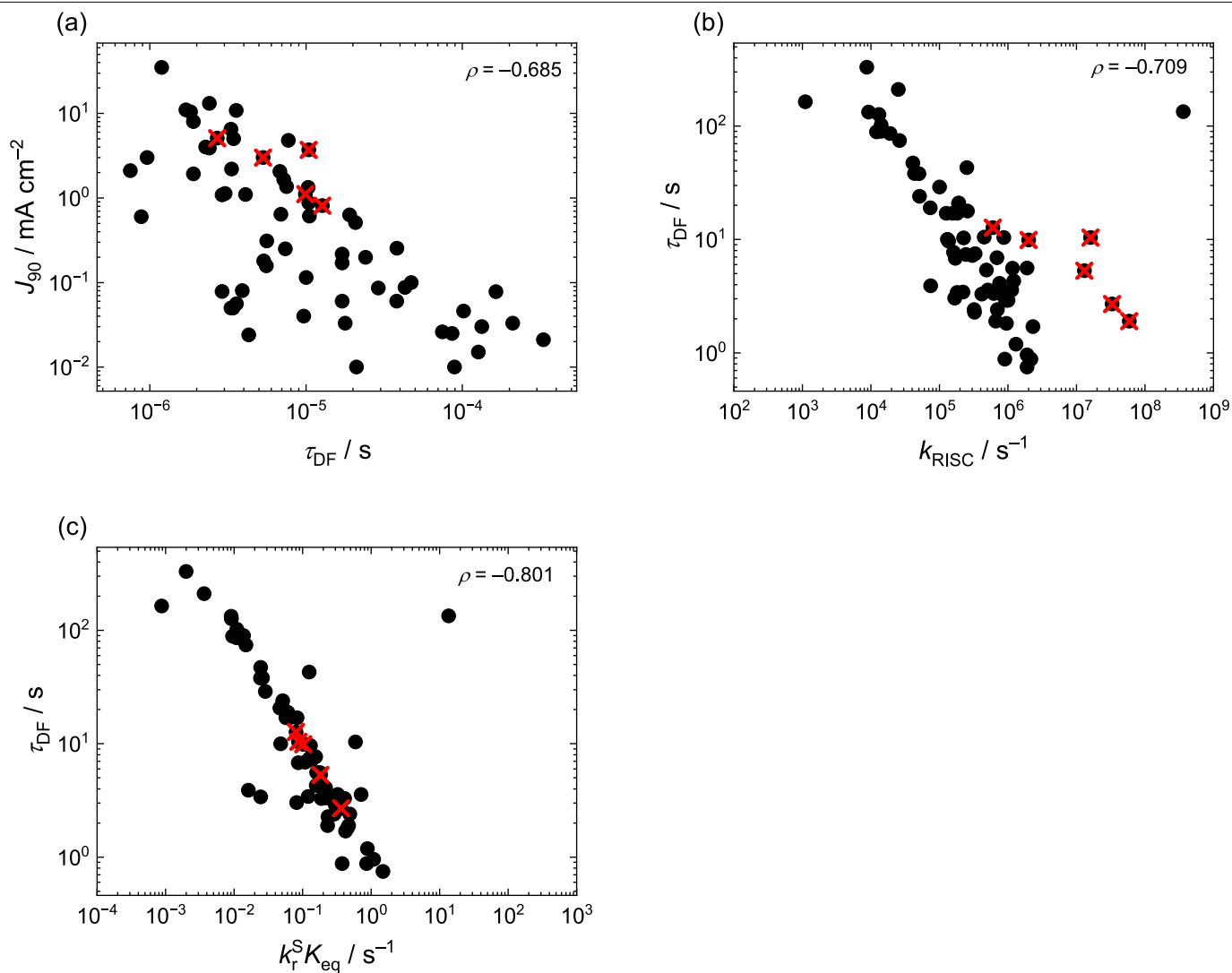
Supplementary information The online version contains supplementary material available at <https://doi.org/10.1038/s41586-024-07149-x>.

Correspondence and requests for materials should be addressed to E. Zysman-Colman or I. D. W. Samuel.

Peer review information *Nature* thanks Hironori Kaji, Xian-Kai Chen and the other, anonymous, reviewer(s) for their contribution to the peer review of this work. Peer reviewer reports are available.

Reprints and permissions information is available at <http://www.nature.com/reprints>.

Analysis

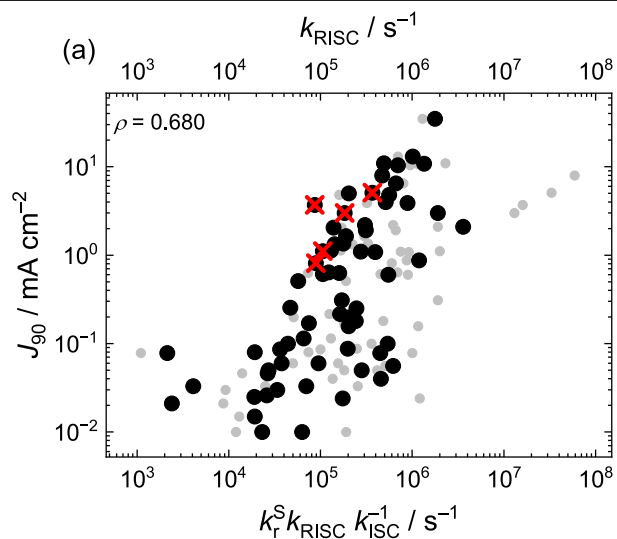


Extended Data Fig. 1 | Correlation with delayed fluorescence lifetime τ_{DF} .

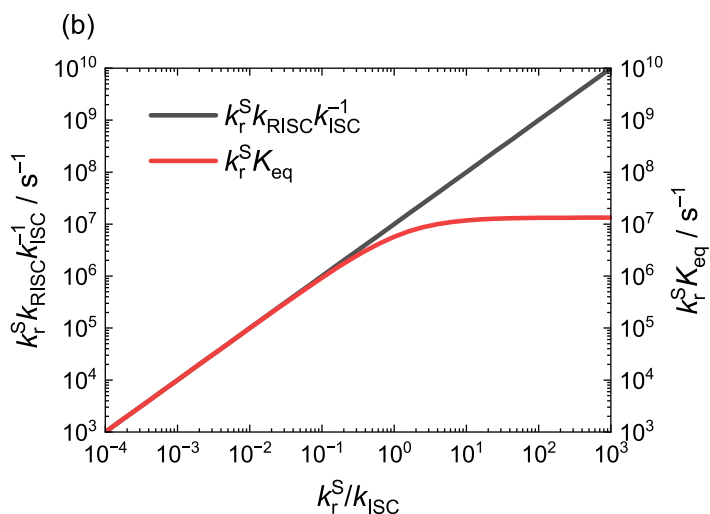
(a) Dependence of J_{90} on τ_{DF} with a Spearman correlation, ρ , of -0.685 .

(b) Dependence of τ_{DF} on k_{RISC} ($\rho = -0.709$). (c) Dependence of τ_{DF} on $k_r^S K_{\text{eq}}$

($\rho = -0.801$). Red crosses identify TADF molecules containing heavy atoms that enhance SOC, which leads to an increase in k_{RISC} .

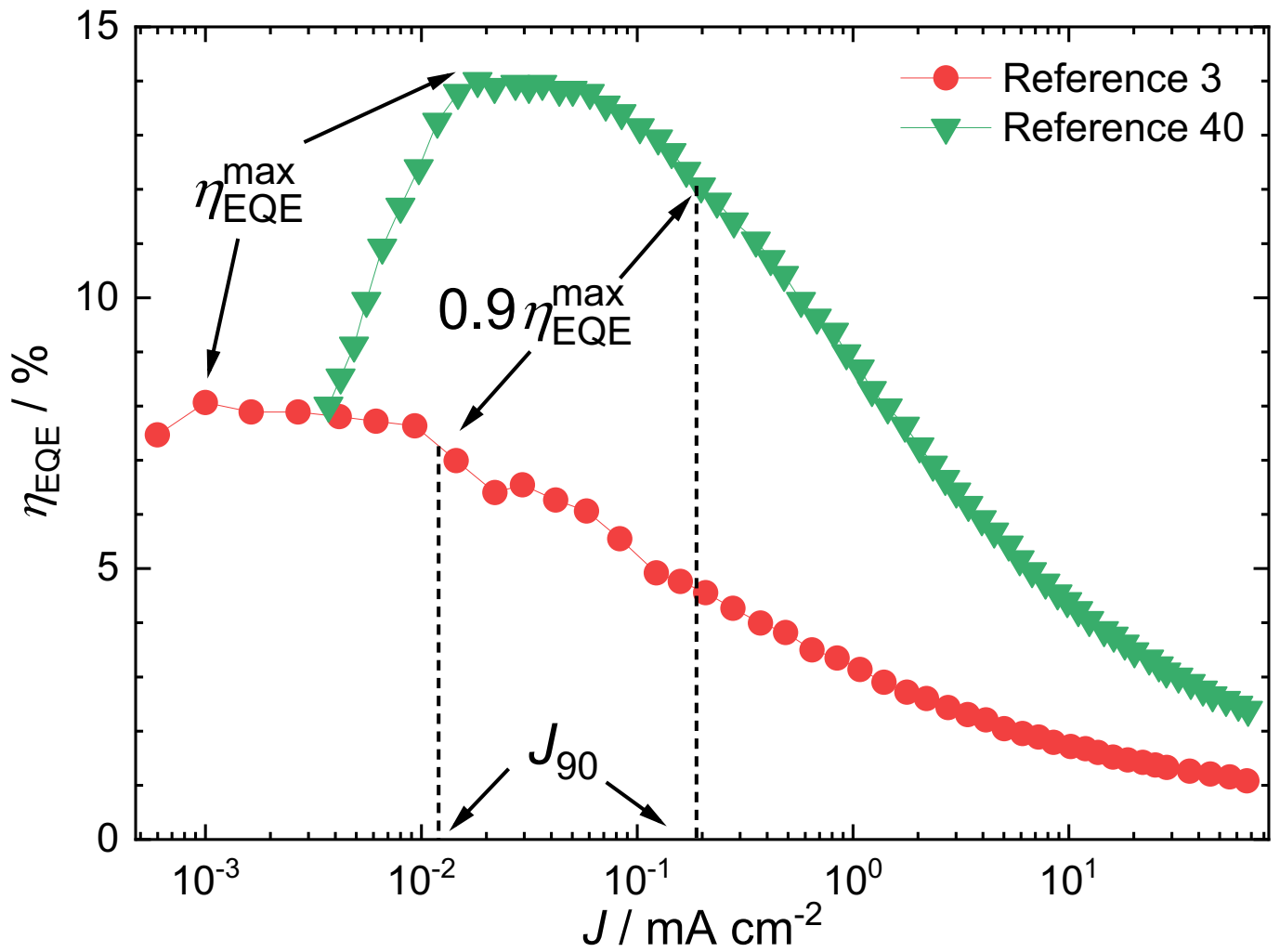


Extended Data Fig. 2 | Simplified Figure of Merit. (a) Correlation between J_{90} and the simplified FOM of $k_r^S k_{\text{RISC}} / k_{\text{ISC}}$ with a Spearman correlation of $\rho = 0.680$, showing a better correlation than k_{RISC} but a less precise predictor than the FOM of $k_r^S K_{\text{eq}}$. Red crosses identify TADF molecules containing heavy atoms that

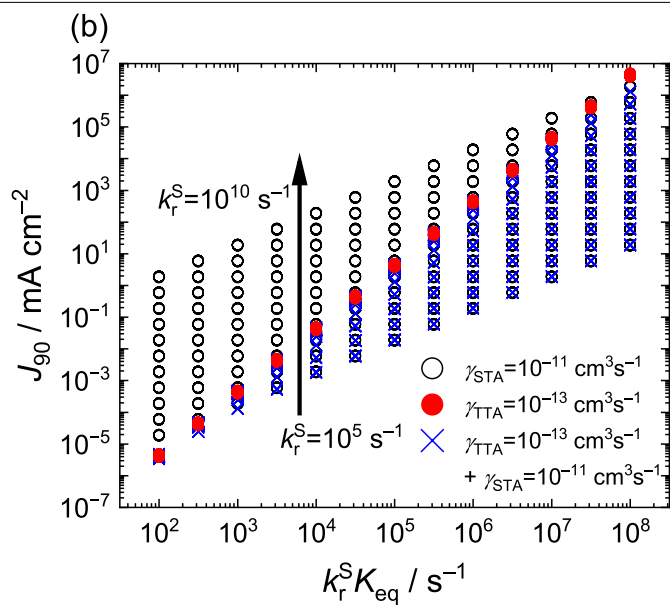
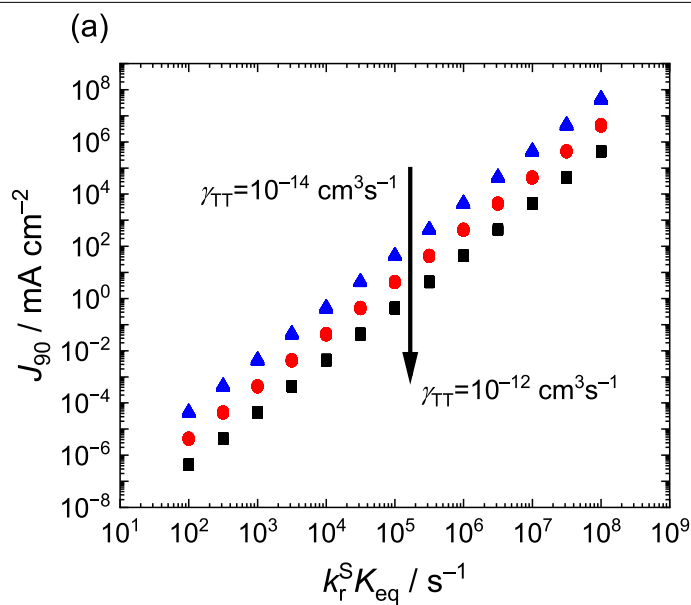


enhance SOC, which leads to an increase in k_{RISC} . In grey circles, the correlation of J_{90} and k_{RISC} from Fig. 3 is displayed for comparison. (b) Deviation between the FOM of $k_r^S K_{\text{eq}}$ and its simplification of $k_r^S k_{\text{RISC}} / k_{\text{ISC}}$ for $k_{\text{RISC}} = 10^7 \text{ s}^{-1}$ showing a deviation between the FOMs for systems with competitive k_r^S and k_{ISC} .

Analysis



Extended Data Fig. 3 | Device influence on Roll-off. Comparison of efficiency roll-off of two literature 2CzPN OLEDs showing different J_{90} because of different efficiency rise at low current densities^{3,40}.



Extended Data Fig. 4 | Impact of STA and TTA on roll-off. The impact of STA and TTA on the correlation between J_{90} and $k_r^S K_{eq}$ calculated for a simplified three-level system with k_r^S between 10⁵ s⁻¹ and 10¹⁰ s⁻¹, k_{ISC}/k_r^S between 10⁻¹ and

10³ and $k_r^S K_{eq}$ between 10² s⁻¹ and 10⁸ s⁻¹ (a) for three different TTA rate constants and (b) for a particular STA rate, a particular TTA rate and a particular combination of STA and TTA rate.

Analysis

Extended Data Table 1 | Parameters for Extended Data Fig. 4

k_r^S (s ⁻¹)	$\frac{k_{ISC}}{k_r^S}$	$k_r^S K_{eq}$ (s ⁻¹)
10 ^{5.0}	10 ^{-1.0}	10 ^{2.0}
10 ^{5.5}	10 ^{-0.5}	10 ^{2.5}
10 ^{6.0}	10 ^{0.0}	10 ^{3.0}
10 ^{6.5}	10 ^{0.5}	10 ^{3.5}
10 ^{7.0}	10 ^{1.0}	10 ^{4.0}
10 ^{7.5}	10 ^{1.5}	10 ^{4.5}
10 ^{8.0}	10 ^{2.0}	10 ^{5.0}
10 ^{8.5}	10 ^{2.5}	10 ^{5.5}
10 ^{9.0}	10 ^{3.0}	10 ^{6.0}
10 ^{9.5}		10 ^{6.5}
10 ¹⁰		10 ^{7.0}
		10 ^{7.5}
		10 ^{8.0}

Generating parameters for the tested set of theoretical emitters shown in Extended Data Fig. 4.